

# COBE Observations of the Cosmic Infrared Background<sup>\*</sup>

E. L. Wright

*UCLA Astronomy, PO Box 951562, Los Angeles CA 90095-1562, USA*

---

## Abstract

The Diffuse InfraRed Background Experiment (DIRBE) on the COsmic Background Explorer (COBE) measured the total infrared signal seen from space at a distance of 1 astronomical unit from the Sun. Using time variations as the Earth orbits the Sun, it is possible to remove most of the foreground signal produced by the interplanetary dust cloud [zodiacal light]. By correlating the DIRBE signal with the column density of atomic hydrogen measured using the 21 cm line, it is possible to remove most of the foreground signal produced by interstellar dust, although one must still be concerned by dust associated with H<sub>2</sub> (molecular gas) and H II (the warm ionized medium). DIRBE was not able to determine the Cosmic InfraRed Background (CIRB) in the 5-60  $\mu\text{m}$  wavelength range, but did detect both a far infrared background and a near infrared background. The far infrared background has an integrated intensity of about 34 nW/m<sup>2</sup>/sr, while the near infrared and optical extragalactic background has about 59 nW/m<sup>2</sup>/sr. The Far InfraRed Absolute Spectrophotometer (FIRAS) on COBE has been used to constrain the long wavelength tail of the far infrared background but a wide range of intensities at 850  $\mu\text{m}$  are compatible with the FIRAS data. Thus the fraction of the CIRB produced by SCUBA sources has large uncertainties in both the numerator and the denominator.

*Key words:* cosmic background;infrared

---

## 1 Introduction

The Diffuse InfraRed Background Experiment (DIRBE) on the COsmic Background Explorer(COBE) satellite was designed to measure the Cosmic Infrared Background (CIRB). The results from the DIRBE team's analysis of

---

<sup>\*</sup> The COBE datasets were developed by the NASA Goddard Space Flight Center under the guidance of the COBE Science Working Group and were provided by the NSSDC.

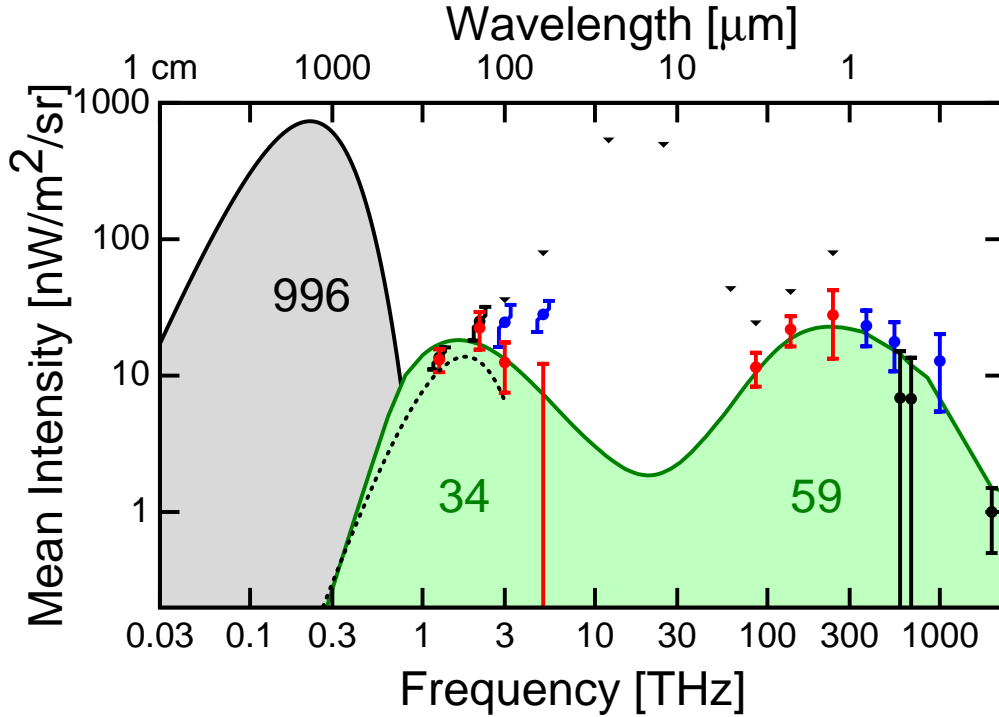


Fig. 1. The Cosmic Infrared and Optical Background from foreground subtracted total intensity measurements only. Black points and upper limits at  $\lambda > 1 \mu\text{m}$  are from (9), while the black points at shorter wavelengths are from (3; 16; 10). The blue points at long wavelengths are from (5), and at short wavelengths from (1). The numbers in the bumps indicate the integrated intensity in  $\text{nW}/\text{m}^2/\text{sr}$  within each bump.

the DIRBE data are described in (9). These depend in a very fundamental way on the model for the zodiacal or interplanetary dust cloud that was fit to the variation of the DIRBE signal as a function of solar elongation (11). But this zodiacal model leaves a large residual intensity at  $25 \mu\text{m}$  which must be due to underestimating the zodiacal background, at least at  $25 \mu\text{m}$ . New models (17; 8) which address this problem are used here to derive new lower values for the CIRB.

Other approaches (5) that use only a small fraction of the DIRBE data to derive a zodiacal model have given higher values for the CIRB. These results are unlikely to be true, but the dominant systematic uncertainty in deriving the CIRB from observations taken 1 AU from the Sun remains the uncertainty in fitting the zodiacal light.

Table 1  
DIRBE Derived CIRB Values

$\lambda$ [ $\mu\text{m}$ ]	$\lambda I_\lambda$ [ $\text{nW}/\text{m}^2/\text{sr}$ ]		
	This paper	FDS	Hauser <i>et al.</i>
1.25	$28 \pm 15$	–	$< 75$
2.2	$22 \pm 6$	–	$< 39$
3.5	$11.5 \pm 3.2$	–	$< 23$
60	$-8 \pm 14$	$28.1 \pm 7$	$< 75$
100	$12.5 \pm 5$	$24.6 \pm 8$	$< 38$
140	$22 \pm 7$	–	$25 \pm 6.9$
240	$13 \pm 2.5$	–	$13.6 \pm 2.5$

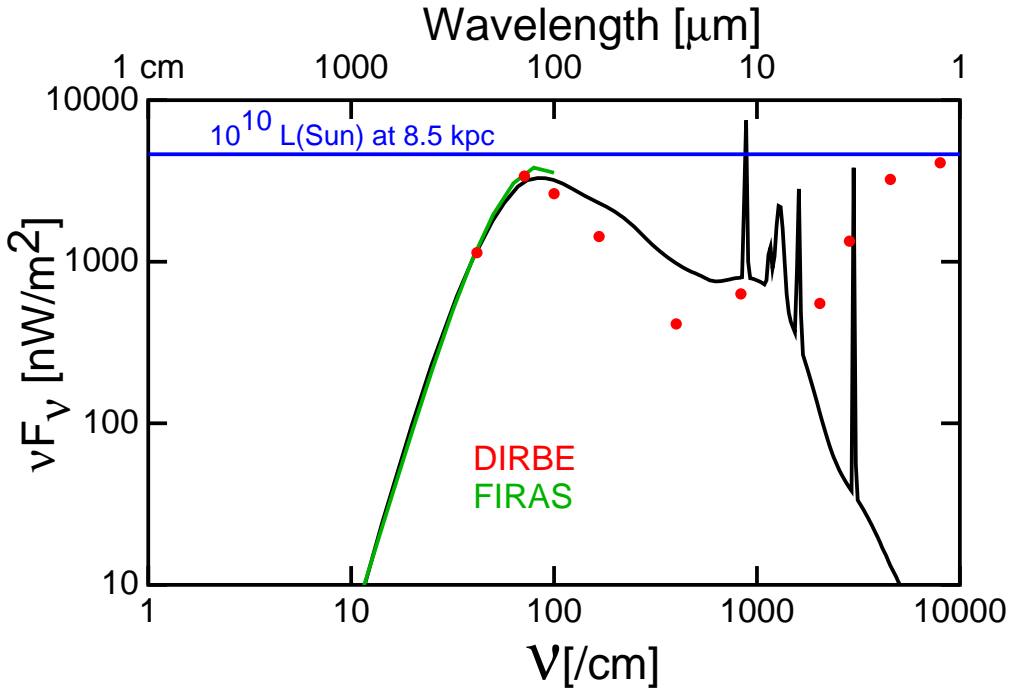


Fig. 2. Milky Way fluxes measured by FIRAS and DIRBE on COBE. The black curve is the dust model from (4) for  $\log(L/L_\odot) = 10.25$  at 8.5 kpc distance.

## 2 The CIRB

The DIRBE team zodiacal light model (11) leaves nearly 2 MJy/sr at 25  $\mu\text{m}$  in dark regions of the sky. This is about 6% of the zodiacal signal, and gives a reasonable estimate of the uncertainty in the zodiacal modeling. This residual intensity corresponds to about 1 photon/ $\text{cm}^3/\text{octave}$ . The lack of a huge  $\gamma$ -ray absorption at 10 TeV energy implies that most of this residual intensity is in fact due to errors in modeling the zodiacal light. If I add a

Table 2  
DIRBE Derived Milky Way Fluxes

$\lambda$ [ $\mu\text{m}$ ]	$\lambda F_\lambda$ [ $\mu\text{W}/\text{m}^2$ ]	$F_\nu$ [MJy]
1.25	4.10	1.71
2.2	3.23	2.37
3.5	1.34	1.56
4.9	0.55	0.90
12	0.63	2.53
25	0.41	3.43
60	1.43	28.6
100	2.64	87.9
140	3.39	158.
240	1.14	90.9

requirement that the mean high galactic latitude residual intensity should be zero to the standard DIRBE zodiacal light modeling, then I get a model (8) with a different geometrical shape for the zodiacal cloud which gives different estimates for the zodiacal light in all DIRBE bands, not just the 25  $\mu\text{m}$  band. Using these new estimates for the zodiacal light, the value of the estimated CIRB at 100  $\mu\text{m}$  changes from  $20 \pm 5 \text{ nW}/\text{m}^2/\text{sr}$ , which was only quoted as an upper limit in (9), to the lower values given in Table 1 and shown on Figure 1. This change has a moderate effect on the estimated 140  $\mu\text{m}$  CIRB as well, but very little effect at 240  $\mu\text{m}$ .

Using a statistical argument (18) or ground-based observations (8; 19) to remove the galactic foreground stars allows one to derive estimates instead of upper limits in the short wavelength bands. The net result is a CIRB with nearly twice as much energy in the near infrared and optical bump as in the far infrared bump. The very common statement that the far infrared CIRB is larger than the near infrared and optical CIRB is an error caused by using the *lower limits* given by source counts as actual intensities. Optical work (1) shows the same effect: the measured background is about twice the lower limit derived from source counts. This is presumably due to the faint fuzzy edges of galaxies being missed in total flux calculations (20).

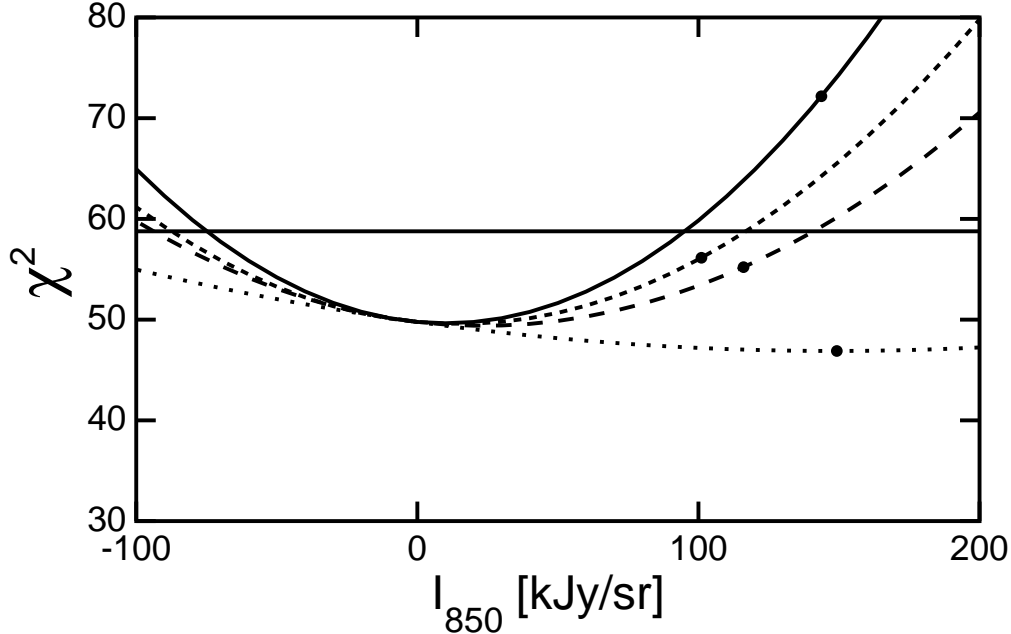


Fig. 3.  $\chi^2$  for the FIRAS low frequency channel data as function of the 850  $\mu\text{m}$  intensity for four different models: solid (7), long dashed (12), short dashed is a  $\nu^2$  power law (14), and the dotted curve is a scaled  $\Lambda\text{CDM}$  Salpeter IMF model (13) which I have modified to be consistent with the FIRAS data. The dot indicates the position for the published normalization. The horizontal line is drawn at  $\Delta\chi^2 = 9$  units above the no-CIRB  $\chi^2$ .

### 3 Milky Way Flux

One quantity easily derivable from the DIRBE and FIRAS maps is the flux of the Milky Way. There is some ambiguity due to the fact that we are located inside the Milky Way, but the definition of the flux is easy to compute:

$$F_\nu = \int \int I_\nu(l, b) \cos l \cos b d\Omega. \quad (1)$$

This is tabulated in Table 2 and plotted in Figure 2. Note that the power in the near infrared is slightly larger than in the far infrared. This is significant since the exactly edge-on orientation of the Milky Way in our sky strongly suppresses the near infrared flux. Thus the Milky Way has a much larger luminosity  $\nu L_\nu$  in the near infrared than the far infrared. Galaxies near  $L_*$  such as the Milky Way should dominate the integrated extragalactic background light, so the fact that the near infrared bump in the CIRB is larger than the far infrared bump is easily understood.

Table 3  
Model CIRB Curve

$\log(\lambda [\mu\text{m}])$	$\log(\lambda I_\lambda [\text{nW}/\text{m}^2/\text{sr}])$	$\log(\lambda [\mu\text{m}])$	$\log(\lambda I_\lambda [\text{nW}/\text{m}^2/\text{sr}])$
-7.921	-1.921	1.154	0.269
-4.523	-1.046	1.270	0.298
-0.824	0.176	1.445	0.446
-0.451	0.985	1.980	1.102
-0.287	1.164	2.150	1.231
-0.076	1.321	2.265	1.261
0.107	1.358	2.384	1.227
0.234	1.336	2.476	1.151
0.375	1.239	2.576	1.003
0.525	1.052	2.676	0.704
0.891	0.474	3.376	-2.122
1.037	0.317	5.276	-10.250

#### 4 FIRAS Limits on the sub-mm Background

The final analysis (6) of the FIRAS low frequency channel data on the Cosmic Microwave Background (CMB) showed a spectrum with rms residuals from a blackbody of 50 ppm of the peak, or 20 kJy/sr. How is this result compatible with SCUBA results that claim to see an integrated intensity from source counts of 86 kJy/sr (15)? One explanation is that later more extensive observations (2) give lower source counts and  $\int SdN = 46$  kJy/sr for  $S > 2$  mJy. A second explanation is that the FIRAS analysis for CMB distortions was designed to be insensitive to any foreground that had the spectral shape of the Milky Way. Thus the CIRB at 850  $\mu\text{m}$  can be quite large if the CIRB spectrum is similar to the Milky Way spectrum.

Equation (3) from (6) gives this model for small deviations of the CMB from a blackbody:

$$I_0(\nu) = B_\nu(T_0) + \Delta T \frac{\partial B_\nu}{\partial T} + G_0 g(\nu) + p \frac{\partial S_c}{\partial p} \quad (2)$$

where  $p$  describes some distortion. In order to see how compatible different models for the cosmic sub-mm background are with the FIRAS low frequency

channel data, I compute the following:

$$\chi^2(p) = \min_{\Delta T, G_0} \left[ \sum_{\nu, \nu'} (I_0(\nu) - p \frac{\partial S_c}{\partial p}) [C^{-1}]_{\nu, \nu'} (I_0(\nu') - p \frac{\partial S_c}{\partial p}) \right], \quad (3)$$

with  $C_{\nu, \nu'}$  being the covariance matrix, and let  $p$  be the sub-mm background intensity at  $850 \mu\text{m}$ , while  $S_c$  gives the shape of the spectrum. Thus  $\partial S_c / \partial p$  is the spectrum normalized to the  $850 \mu\text{m}$  value. Figure 3 shows the  $\chi^2$  vs.  $I_{850}$  curves for four different models of the sub-mm background. The two models with the high values of  $I_{850}$  have the best and the worst  $\chi^2$ , while the models with lower intensities at  $850 \mu\text{m}$  have marginal  $\chi^2$ 's. The model with the highest  $\chi^2$  is the analytic fit  $I_\nu = 1.3 \times 10^{-5} (100 \mu\text{m} / \lambda)^{0.64} B_\nu(18.5 \text{ K})$  from (7), but this model was designed to fit the peak of the CIRB near  $200 \mu\text{m}$ , and not the faint low SNR region near  $850 \mu\text{m}$ . Table 3 gives the values of  $\lambda I_\lambda$  vs.  $\lambda$  for the model with the best  $\chi^2$  in Figure 3. I designed the shape of this model near  $850 \mu\text{m}$  to make it compatible with the FIRAS limits. This is also the curve shown in Figure 1. Clearly more work is needed to determine  $I_{850}$ , and this requires a better indicator of the total galactic column density including all types of matter: H I, H II, and H<sub>2</sub>.

## 5 Discussion

I have presented here results from the DIRBE and FIRAS observations of the CIRB and the Milky Way. Both the Milky Way and the CIRB show a bigger peak in the near infrared than in the far infrared. The total intensity is nearly 10% of the power in the CMB blackbody. While the CIRB is probably the integrated light from many unresolved galaxies, there is a discrepancy between galaxy photometry and the near infrared and optical CIRB, with the directly measured CIRB being about two times brighter than the intensity from source counts. The most probable explanation of this discrepancy is undercounting the faint outer parts of galaxies.

## References

- [1] Bernstein, R., Freedman, W. & Madore, B., *Astrophysical Journal* **571**, (2002) 56.
- [2] Borys, C., Chapman, S., Halpern, M. & Scott, D., *MNRAS* in press, astro-ph/0305444.
- [3] Dube, R. R., Wicks, W. C. & Wilkinson, D. T., *Astrophysical Journal Letters* **215** (1977) L51.

- [4] Dwek, E., Arendt, R. G., Hauser, M. G., Fixsen, D., Kelsall, T., Leisawitz, D., Pei, Y. C., Wright, E. L., Mather, J. C., Moseley, S. H., Odegard, N., Shafer, R., Silverberg, R. F. & Weiland, J. L., *Astrophysical Journal* **508** (1998) 106.
- [5] Finkbeiner, D., Davis, M. & Schlegel, D., *Astrophysical Journal* **544** (2000) 81.
- [6] Fixsen, D. J., Cheng, E. S., Gales, J. M., Mather, J. C., Shafer, R. A. & Wright, E. L., *Astrophysical Journal* **473** (1996) 576.
- [7] Fixsen, D., Dwek, E., Mather, J. Bennett, C. & Shafer, R., *Astrophysical Journal* **508** (1998) 123.
- [8] Gorjian, V., Wright, E. & Chary, R., *Astrophysical Journal* **536** (2000) 550.
- [9] Hauser, M. G., Arendt, R. G., Kelsall, T., Dwek, E., Odegard, N., Weiland, J. L., Freudenreich, H. T., Reach, W. T., Silverberg, R. F., Moseley, S. H., Pei, Y. C., Lubin, P., Mather, J. C., Shafer, R. A., Smoot, G. F., Weiss, R., Wilkinson, D. T. & Wright, E. L., *Astrophysical Journal* **508** (1998) 25.
- [10] Hurwitz, M., Bowyer, S. & Martin, C., *Astrophysical Journal* **372** (1991) 167.
- [11] Kelsall, T., Weiland, J. L., Franz, B. A., Reach, W. T., Arendt, R. G., Dwek, E., Freudenreich, H. T., Hauser, M. G., Moseley, S. H., Odegard, N. P., Silverberg, R. F. & Wright, E. L., *Astrophysical Journal* **508** (1998) 44.
- [12] Lagache, G., Abergel, A., Boulanger, F., Desert, F. X. & Puget, J. L., *Astronomy & Astrophysics*, **344** (1999) 322.
- [13] Primack, J., Bullock, J., Somerville, R. & MacMinn, D., *Astroparticle Physics* **11** (1999) 93.
- [14] Puget, J.-L., Abergel, A., Bernard, J.-P., Boulanger, F., Burton, W., Désert, F.-X. & Hartmann, D., *Astron. Astrophys.* **308** (1996) 5.
- [15] Smail, I., Ivison, R., Blain, A. & Kneib, J.-P., *astro-ph/9810281* (1998).
- [16] Toller, G. N., *Astrophysical Journal Letters* **266** (1983) L79.
- [17] Wright, E. L., *Astrophysical Journal* **496** (1998) 1.
- [18] Wright, E. & Reese, E., *Astrophysical Journal* **545** (2000) 43.
- [19] Wright, E. & Johnson, B. *astro-ph/0107205* (2001).
- [20] Wright, E. L., *Astrophysical Journal Letters* **556** (2001) L17.